Medical Stents: State of the Art and Future Directions

Development of a Novel Biodegradable Metallic Stent Based on Microgalvanic Effect

Jennifer Frattolin,[1,2] Rajib Barua,[1] Huseyin Aydin,[4] Sriraman Rajagopalan,[4] Luca Gottellini,[1,5] Richard Leask,[3] Stephen Yue,[4] David Frost,[1] Olivier F. Bertrand,[1,6] and Rosaire Mongrain[1,2,7]

[1]Department of Mechanical Engineering, McGill University, Montreal, QC, Canada; [2]Montreal Heart Institute, Montreal, QC, Canada; [3]Department of Chemical Engineering, McGill University, Montreal, QC, Canada; [4]Department of Mining and Materials Engineering, McGill University, Montreal, QC, Canada; [5]Department of Chemistry, Materials and Chemical Engineering, Politecnico di Milano, Milan, Italy; [6]Interventional Cardiology Laboratories, Quebec Heart and Lung Institute, Laval University, Quebec City, QC, Canada; and [7]McGill University, Macdonald Engineering Building, Room 369, 817 rue Sherbrooke Ouest, Montreal, QC H3A 0C3, Canada

Associate Editor Abdul I. Barakat oversaw the review of this article.

Abstract—The implementation of biodegradable stents has the potential to revolutionize obstructive coronary artery disease treatment. Limitations still currently exist, however, that prevent biodegradable stents from replacing permanent metallic stents in the global market. The ideal combination of stent properties, including sufficient mechanical strength, controlled degradation, and biocompatibility, has yet to be realized. A novel manufacturing process is proposed that utilizes cold gas-dynamic spraying to fabricate a metal structure with significantly reduced grain size. Iron and stainless steel 316L are combined to form a novel amalgamate with enhanced mechanical strength and a controllable degradation rate, due to the resulting microgalvanic reaction. Flat specimens composed of iron and 316L are fabricated in various compositions, and mechanical and degradation tests were conducted. Femto laser techniques are utilized to produce stents composed of 80% Fe and 20% stainless steel 316L. The *in vitro* degradation behaviour of the stent is investigated using static and dynamic corrosion tests. It is shown that the corrosion rate can be adjusted to desired values, by varying the weight percentage of iron and stainless steel 316L within the amalgamate.

Keywords—Biodegradable stent, Microgalvanic corrosion, Cold spray, Coronary artery disease, Degradation.

INTRODUCTION

The design of a coronary stent has gone through several iterations since the inception of the Palmaz-Schatz stent in 1986.[6] The current trend in stent design has seen a shift from permanent stents to the implementation of novel biodegradable materials.[26,31] There are still remaining challenges, however.[14] The current generation of polymer-based biodegradable stents has significantly lower mechanical properties in comparison to permanent metallic stents, resulting in larger strut thickness to limit elastic recoil and ensure sufficient radial strength.[25] Thicker stent struts, however, may be associated with acute stent thrombosis or late in-stent restenosis.[19,20] In addition, the late effects of polymer degradation products on vascular tissue remain largely unknown.[17]

As a result, two degradable metals have come to the forefront of biodegradable stent research: magnesium and iron. The benefit of utilizing metallic alloys is the ability to exploit their oxidative properties for degradation. It was for this reason that the principle material investigated was magnesium.[15] Like polymers, however, magnesium has elastic and tensile properties that are much lower than current metallic alloys and thicker struts are therefore required.[26]

In comparison to magnesium, iron-based alloys have greater tensile and yield strength, as well as greater ductility.[9] Statistical size effects (SSEs), however, are problematic with newly developed iron-manganese alloys, as its average grain size is relatively

large, typically around 100 μm.[8,13] SSEs are characterized by few grains in one spatial direction, which have a weakening contribution to the component's mechanical strength.[10,11,22] In contrast, electroformed iron has improved grain size (2–8 μm), thus limiting potential complications due to SSEs, but possesses limited ductility (approximately 18%).[27] Other combinations, such as Fe–Au and Fe–Ag, are also currently under development.[16]

To alleviate the limitations of current biodegradable stents, a novel manufacturing approach is proposed to fabricate a material of reduced grain size for biodegradable stent application. A fine microstructure is critical to stent success given the current trend of minimizing strut thickness. Achieving a reduced grain size can be difficult in stent design, however, as conventional methods cannot be employed. Such techniques, like cold-working, make the material too brittle for stent application.[7]

In the proposed design, cold gas dynamic spraying (CGDS) is used to generate an improved stent material with smaller grains. The cold spray process utilizes the energy stored in high-pressure gas to propel micron-sized particles of powder at high velocities (300–1500 m s^{-1}). The high pressure gas, characteristically nitrogen or helium, is pre-heated, and fed through the powder feeder, which introduces the powder into the gas jet stream (Fig. 1a).[1] Since the powder impacts the substrate at a high velocity, the particles deform, adhere to the substrate and form a coating. During this process, the temperature of the powder remains relatively low (gas temperature ranges between 100 and 800 °C).[1] Unwanted effects due to a change in the powder's thermal environment are avoided, including oxidation, thermal stresses, and grain growth. No melting is observed, and the particles are able to yield and mix under very high strain rates, producing a complex microstructure.[1] The resulting microstructure has grain sizes in the micron to submicron range, leading to increased strength and fatigue resistance, as well as excellent wear properties.[28]

Therefore, utilizing cold spray technology, a novel biodegradable stent is proposed, composed of an intermixed composite material of stainless steel 316L and pure iron. Current iron-based biodegradable stents are associated with complications resulting from poor ductility and SSEs.[10] The proposed invention exploits the advantageous reduction in grain size observed with CGDS, thereby eliminating complications associated with SSEs, while allowing for high mechanical strength and ductility.

Furthermore, iron (anodic) and stainless steel 316L (cathodic) are dissimilar metals with a large potential difference. By combining the two dissimilar metallic powders, a galvanic couple is induced. The resulting metallic amalgamate after CGDS has a controllable degradation rate, by means of the resulting galvanic corrosion reaction. This reaction preferentially corrodes iron at the micro-scale, accelerating the overall corrosion behaviour of the stent. Moreover, it is possible to modify and control the corrosion rate by adjusting the relative weight percentages of iron and stainless steel 316L. This is particularly advantageous for biodegradable stents, as obtaining a controlled degradation is critical to its successful implementation in a clinical setting.

In the subsequent sections, the fabrication techniques utilized to manufacture the proposed biodegradable stent through CGDS are explained, and the results of preliminary material testing of the novel Fe-316L amalgamate are presented, including mechanical and selected corrosion tests.

MATERIALS AND METHODS

The fabrication procedure proposed in the subsequent sections was a result of optimizing the cold spray process for stent application, including powder selection and cold spray parameters, as well as investigating and improving the corrosion and mechanical behaviour. Further details regarding this iterative process are presented in Mongrain et al.,[24] Barua,[5] and Al-Mangour.[1]

Statistical analysis of the data sets was completed in GraphPad Prism 5.01 (GraphPad Software Inc., La Jolla, CA, USA). One and Two Way ANOVA's were used to compare the data with Bonferroni's Multiple Comparison Test. A p value of less than 0.05 was considered significant.

Flat Specimen Fabrication

Cold Gas Dynamic Spray Process

Commercially available stainless steel 316L powder (SandVik Osprey, UK), with a particle size of 43.7 ± 17 μm, and 99% pure iron powder (SandVik Osprey, UK), with a particle size of 25.2 ± 14.6 μm, were mixed (Fig. 2). Particle size distribution was measured by a LA-920 laser diffraction analyzer (HORIBA Scientific, France). Powder was prepared in different ratios, quantified by the nominal concentration of iron and stainless steel 316L. Combinations of powder were prepared in the following mixtures: 20Fe-80SS, 50Fe-50SS, and 80Fe-20SS, where the numbers indicate the powder's weight percentage, as well as pure iron (100Fe) and 316L. A rolling mixer was used to mix the powders for 1 h. The chemical composition of the prepared powders, measured by inductive coupled plasma mass spectrometry (ICP-MS), is presented in Table 1.
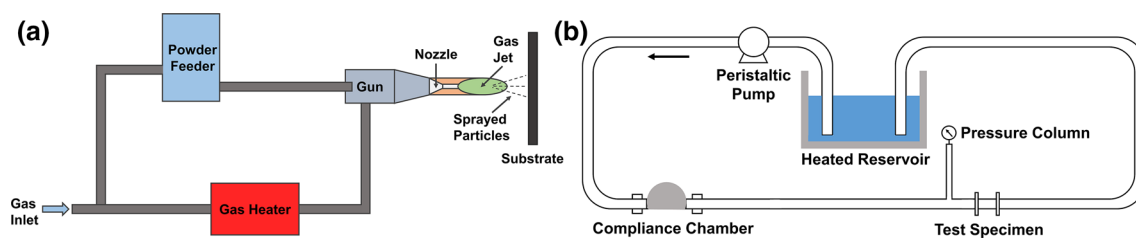
FIGURE 1. (a) Schematic diagram of the cold spray system utilized to fabricate the novel metallic amalgamate. Preheated high-pressure gas propels micron-sized particles of powder at high velocities, characteristically 300–1500 m s^{-1}. The powder hits the substrate, causing the particles to deform, adhere to the substrate and form a coating. (b) Schematic diagram of the dynamic corrosion test bench. A peristaltic pump, as well as compliance chamber, was utilized to implement flow consistent with that in the coronary arteries. A heated reservoir was used to maintain solution temperature at 37 °C.
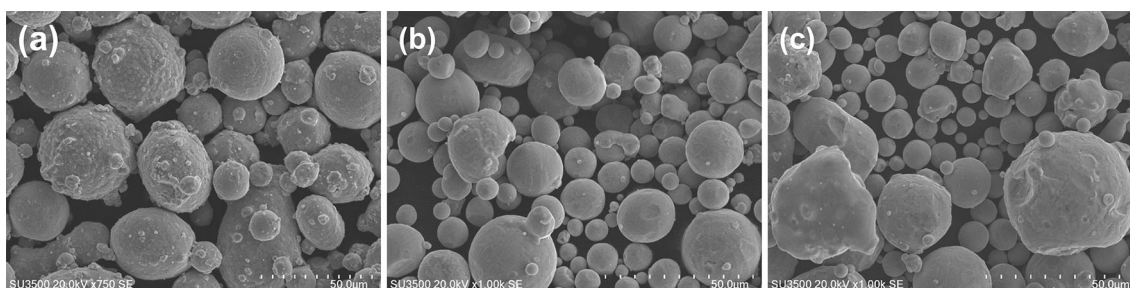

FIGURE 2. Characterization of the metallic powders was performed by scanning electron microscopy (SEM). (a) Pure stainless steel 316L powder, (b) pure iron powder, and (c) a powder mixture containing 80% iron powder and 20% stainless steel 316L powder. The particles of iron and stainless steel 316L are uniformly distributed, as the powders are mixed for 1 h in a rolling mixer.

The Kinetiks® 4000 cold spray system (Oerlikon Metco, Switzerland) was utilized, with nitrogen gas (N$_2$) as the propellant at 700 °C and at a pressure of 4 MPa. Coatings were sprayed onto 1020 cold-rolled steel plates (100 mm × 100 mm × 3 mm). The substrates were grit-blasted prior to deposition for increased coating adhesion. Coating thickness was approximately 1 mm.

Heat Treatment and Post-Processing

After spraying, the coated substrates were annealed at 1100 °C for 1 h in a temperature-controlled box furnace (ThermCraft, Winston-Salem, USA). Argon gas was utilized to minimize coating oxidation. The sample was cooled within the furnace before removal. The specimens were ground to reduce coating thickness, and electrical discharge machining (EDM) was utilized to cut the specimens into the desired dimensions, and separate the substrate from the coating.[1,2]

Flat Specimen Testing

Chemical Composition and Microstructure

The microstructure of the amalgamates was characterized after heat treatment using optical micro-

scopy. Specimens composed of 20Fe-80SS, 50Fe-50SS, and 80Fe-20SS were analyzed, and compared to a non-annealed 80Fe-20SS sample. Porosity was assessed with a Nikon® Epiphot 200 microscope (Nikon Instruments Inc., Melvile, NY, USA), with Clemex© Vision software (Clemex Technologies Inc., Longueuil, QC, Canada). Porosity measurements were conducted at 200× magnification, with 20 measurements recorded for each specimen.

To investigate the grain size of the proposed manufacturing technique, electron backscatter diffraction (EBSD) was conducted utilizing scanning electron microscopy (SEM) to analyze the grain size of a 316L specimen.

Static Corrosion Test

Static corrosion tests were conducted according to ASTM Standard G31-12a.[3] Five different specimens (10 mm × 20 mm) were prepared: 316L, 20Fe-80SS, 50Fe-50SS, 80Fe-20SS, and 100Fe. The experiments were repeated in triplicate. Samples were immersed in a 2 L reaction beaker prepared with modified HyClone™ Hanks' Balanced Salt Solution (HBSS) (Fisher Scientific, Canada), as its ionic composition is similar to that of blood plasma. In order to preserve the physiological pH (approximately 7.4), the solution

TABLE 1. Chemical composition of the prepared powders in relative weight percentage.

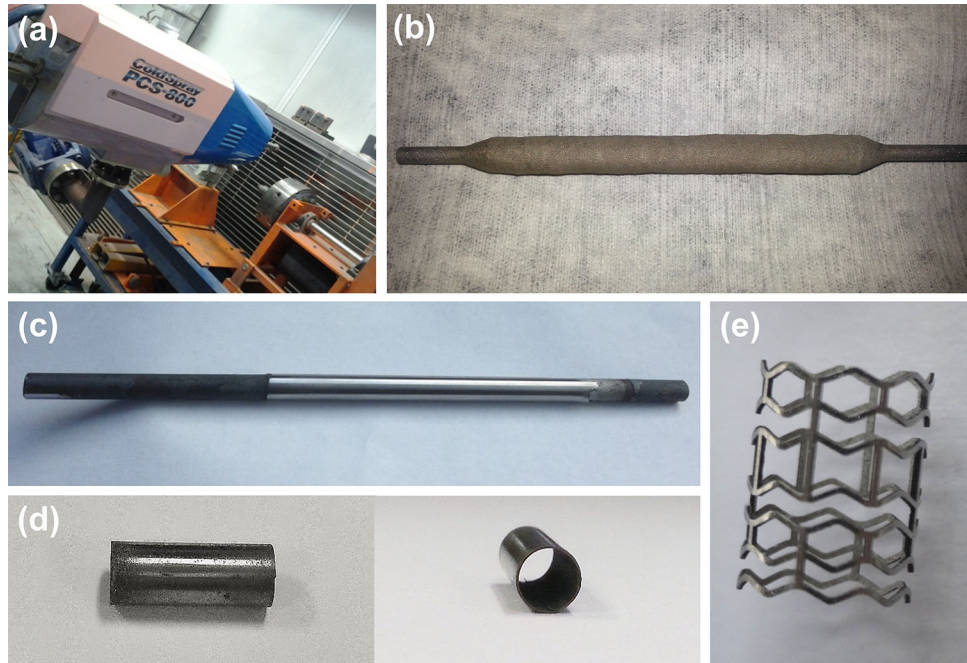| Sample	Fe	Cr	Ni	Mo	Mn	Si	C
316L	68.70	16.24	10.93	2.200	1.430	0.436	0.057
20Fe	73.16	13.93	9.391	1.896	1.261	0.316	0.039
50Fe	83.29	9.184	6.222	0.125	0.951	0.194	0.040
80Fe	91.75	4.055	2.793	0.565	0.615	0.170	0.051
100Fe	99.23	0.068	0.123	0.0398	0.369	0.102	0.068

FIGURE 3. Stent fabrication is a five-step process: First, cold-gas dynamic spraying creates a coating on a cylindrical substrate. (a) The Plasma Giken® cold spray system is utilized for coating manufacture. (b) The resulting coated substrates, with a coating thickness of approximately 2 mm radially. (c) Centreless grinding is utilized to reduce coating thickness to 250 μm, while also creating a polished surface. (d) Electric discharge machining (EDM) separates the coating from the substrate, yielding tubes with an inner diameter of 5 mm and an approximate thickness of 250 μm. (e) The completed stent, after femto laser cutting of the stent design and subsequent electropolishing.

was buffered with HEPES.[33] The volume to surface area ratio (V/S) was 34.9 mL cm^{-2}, within the minimum range of 20–40 mL cm^{-2} set by ASTM. The solution was maintained at 37 ± 1 °C, with the temperature and pH monitored throughout the duration of the experiment. The specimens were removed from the test bench every seven to nine days, after which they were cleaned and weighed, for a total test period of 45 days. The corrosion rate of the flat specimens (CR$_{flat}$), in mm year^{-1}, was calculated from Faraday's Law using the following equation:

$$CR_{flat} = \frac{KW}{ADt} \quad (1)$$

where K is a constant, W is the mass loss in grams (g), A is the surface area in cm^2, D is the density in g cm^{-3}, and t is the total exposure time in hours (h). A constant

equal to 8.76×10^4 was utilized for K, in order to yield the desired units of mm year^{-1}.

Galvanic Corrosion Test

To establish whether the corrosion rate was accelerated due to microgalvanic effect, galvanic corrosion tests were conducted according to ASTM G71-81(2014).[4] Samples composed of 20Fe-80SS, 50Fe-50SS, 80Fe-20SS, and 100Fe were utilized, with a control sample of 316L. A total of three specimens for each mixture were tested. A VersaStat3 potentiostat (Princeton Applied Research, TN, USA) was utilized to induce the galvanic couple. The prepared specimens were used as the working electrode. The area ratio between the working electrode and the other electrode, 316L, was 1:1. Current flow between the working electrode and 316L was measured in order to calculate

the galvanic corrosion rate (CR_{galv}). CR_{galv}, in mg $(cm^2\ day)^{-1}$, was determined by the following equation:

$$CR_{galv} = \frac{W}{At} \qquad (2)$$

where A is the surface area in cm^2, t is the elapsed time in days, and W is the mass loss equal to:

$$W = \frac{MIt}{zF} \qquad (3)$$

where M is the molar mass in mg mol^{-1}, I is the current in Ampere, t is the total time in seconds (s), z is ion valence, and F is Faraday's constant, 96,485.34 C mol^{-1}.

Mechanical Test

Micro shear punch tests were conducted utilizing an MTS hydraulic testing machine. Rectangular flat specimens (10 mm × 4 mm) with a thickness of 0.6–0.85 mm were used, composed of 316L, 20Fe-80SS, 50Fe-50SS, 80Fe-20SS, and 100Fe. A strain rate of 0.06 mm $mm^{-1}\ min^{-1}$ was utilized, with a punch diameter of 1.55 mm. The tests were repeated three times.

Specimen area reduction was calculated utilizing the following equation:

$$\text{Percent Area Reduction} = \left(\frac{D_f}{t}\right)100\% \qquad (4)$$

where D_f is the shear punch failure displacement, in mm, and t is the specimen thickness, in mm.

Stent Fabrication

Cold-Gas Dynamic Spray Process

As a result of the previous material tests, the best tested ratio was selected, and therefore iron and 316L powders were mixed in a 4:1 ratio (80Fe-20SS). After preparation, the powder was placed in a rolling mill mixer, with 2 mill balls, for 1 h. The prepared powder was placed in a vacuum furnace prior to spraying to remove humidity, as excessive humidity may affect coating adhesion to the substrate when spraying.[7]

The Plasma Giken® PCS-800 cold spray system (Plasma Giken Co., Ltd., Japan) was utilized for material fabrication (Fig. 3a). Nitrogen gas (N_2) was used as the propellant, at a pressure of 4.9 MPa, and was heated to 700 °C. Coatings were sprayed on 5 mm diameter cylindrical rods, composed of mild carbon steel. Prior to deposition, the substrates were grit-blasted to increase coating adhesion. The substrates were also preheated with 2 passes of nitrogen gas for

better deposition. Radial coating thickness was approximately 2 mm (Fig. 3b). To avoid oxidation after spraying, specimens were kept under vacuum.

Heat Treatment and Post-Processing

After spraying, the coating was in a highly work-hardened state, with little material ductility.[2] Therefore, the coated substrates were annealed at 1150 °C for 1 h in a Type F21100 tube furnace (Barnstead/ Thermolyne Corporation, Iowa, USA), with flowing argon gas for oxidation control. The specimens were cooled at a controlled rate to room temperature.

The post-processing required for stent fabrication is a 4-step procedure, combining: centreless grinding, EDM, femto-laser cutting, and electropolishing. Centreless grinding was utilized to remove excess material, and produce a polished coating. Coating thickness after this process was approximately 250 μm (Fig. 3c). EDM was utilized to separate the coating from the substrate (Fig. 3d).[1,2] The resulting tubes were cut to lengths of 1.5–2 cm. The tubes were then laser cut with the desired stent cell design, based on the Symbiotech® stent (Fig. 3e).[23] A femto laser was used for the cutting process, in order to avoid the high heat associated with conventional laser cutting. Electropolishing was conducted to improve the surface finish of the stent, which led to a reduction of the stent's strut thickness. The resulting stents were 0.8 cm in length, with a strut thickness of 145 μm (Fig. 3e).

Stent Testing

Static Corrosion Test

A static corrosion test utilizing stent specimens was conducted according to ASTM G31-12a.[3] A 100 mL beaker was prepared with 80 mL of buffered HyClone™ HBSS. The V/S ratio was 68.9 mL cm^{-2}, respecting the minimum value set by ASTM. The solution was maintained at 37 ± 1 °C by means of an ISOTEMP 202 hot water bath (Fisher Scientific, Canada). The pH of the solution was monitored daily. The stent was removed from the test bench every 24 h and weighed, with a total test period of 7 days. The corrosion rate (CR_{static}), in mm $year^{-1}$, was calculated utilizing Eq. (1), with a density of 7.89 g cm^{-3}. The corroded surface was analyzed utilizing SEM. This static corrosion test was a preliminary investigation conducted once.

Dynamic Corrosion Test

A dynamic corrosion test was conducted utilizing the test bench shown in Fig. 1b. A Masterflex© peri-

staltic pump (Cole-Parmer Instrument Co., Illinois, USA) was used to provide flow consistent with that found in the left anterior descending artery. A flow rate of 40 mL min^{-1} was implemented, corresponding to a Reynolds number of approximately 270. Masterflex$^{©}$ Tygon E-LFL Pump Tubing (L/S 24) was selected for the setup, with abrasion-resistant polyurethane tubing (Shore hardness of A70) utilized as the specimen holder for stent insertion and placement. Stent specimens were crimped on an angioplasty balloon, and expanded to the tubing diameter of 4.76 mm at the test site. A buffered HBSS was used to preserve physiological pH. The solution was maintained at 37 ± 1 °C, and the pH was monitored every 24 h. Test duration was 7 days, after which the stent was cleaned and weighed. The corrosion rate ($CR_{dynamic}$), in mm year^{-1}, was calculated utilizing Eq. (1). The stent surface was analyzed using SEM, before and after testing. This dynamic corrosion test was a preliminary study conducted once.

RESULTS

Flat Specimen Testing

Microstructure

Specimens composed of 20Fe-80SS, 50Fe-50SS, and 80Fe-20SS were analyzed under optical microscopy (Fig. 4). A non-heat treated specimen, composed of 80Fe-20SS, was also analyzed for comparison (Fig. 4a). The dark and lighter areas of the images correspond to Fe and 316L particles, respectively. It is well documented that as-sprayed coatings are in a work-hardened state, with incomplete interparticle

bonding, large pores and cracked boundaries.[1] The resulting effect of heat treatment was observed under optical microscopy, with recovery and recrystallization of the work-hardened grains evident.

Reduced porosity was observed for all specimens, due to improved continuous interparticle bonding. Qualitatively, fewer fine cracks and pores were evident in comparison to the non-heat treated specimen. Specimens composed of 50Fe-50SS had the lowest porosity of the samples, with an average porosity of 0.089 ± 0.043%. Samples composed of 20Fe-80SS and 80Fe-20SS had slightly elevated porosity values in comparison to 50Fe-50SS samples, at 0.30 ± 0.11 and 0.31 ± 0.24% respectively. In comparison, the non-heated specimen had a porosity of 0.83 ± 0.29%. There was a significant difference in porosity ($p < 0.0001$, One Way ANOVA) between the heat-treated specimens and the non-heat treated specimen. Only the 20Fe-80SS and 80Fe-20SS heat-treated samples could not be distinguished as significantly different (Bonferroni's Multiple Comparison Test).

The grain size of a specimen composed of 316L was analyzed by an EBSD detector. The resulting image is presented in Fig. 4e. A fine microstructure was observed under high magnification, with grain sizes less than 10 μm. This confirms the feasibility of achieving a microstructure in the micron to submicron range by CGDS.

Static Corrosion Test

Flat specimens were tested to investigate the corrosion rate of various amalgamates. The corroded surface of the samples after immersion can be observed in Fig. 5a, and the resulting mass loss curves are pre-
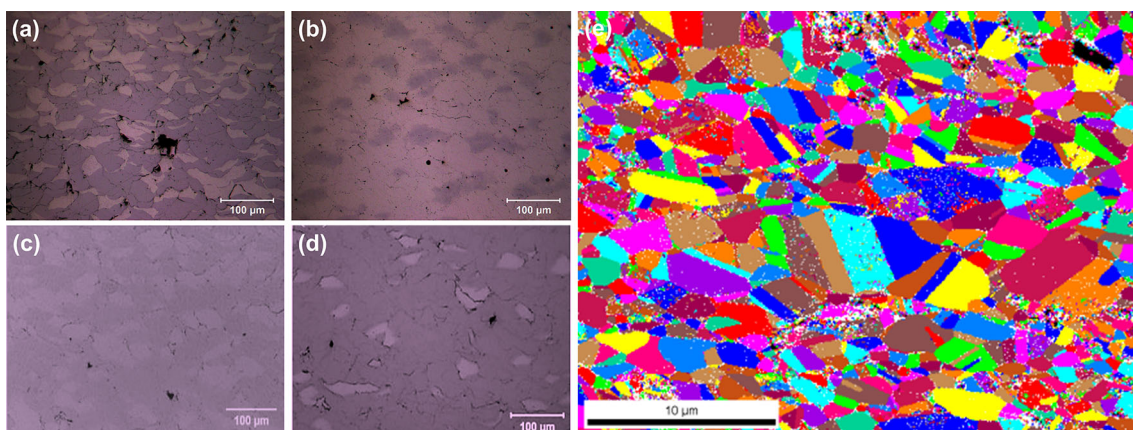

FIGURE 4. Optical microscopy was utilized to analyze the cross sections of flat specimens. (a) First, a non-heat treated specimen composed of 80Fe-20SS was analyzed. Then, individual heat treated specimens were tested, including (b) 20Fe-80SS, (c) 50Fe-50SS, and (d) 80Fe-20SS specimens. The dark and lighter areas of the images correspond to Fe and 316L particles, respectively. In comparison to the non-heat treated specimen, the heat treated specimens' porosity was significantly reduced. (e) To investigate the grain size of the coatings, electron backscatter diffraction (EBSD) was utilized to characterize the grain size of a pure 316L specimen. The average grain size observed was less than 10 μm.
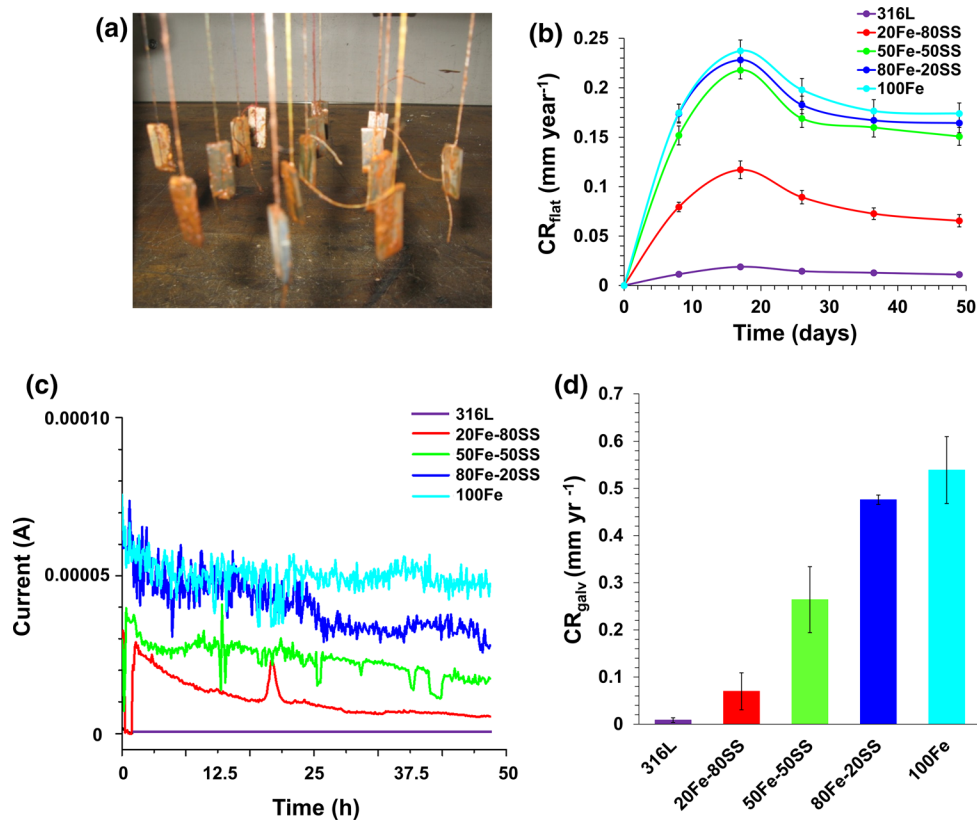
FIGURE 5. (a) The corroded surface of the flat specimens is presented after static corrosion tests. (b) The results of the static corrosion tests, using flat specimens. The resulting curve shows the change of corrosion rate curve, in mm year^{-1}, with respect to time. The tests were completed in triplicate ($n = 3$), and the standard deviation is presented. (c) The output results of the galvanic corrosion test, specifically the current vs. time curve. (d) The calculated galvanic corrosion rate of the different specimens, in mm year^{-1}. Standard deviation was calculated for each powder mixture, with $n = 3$.

sented in Fig. 5b. Initially, there was a rapid increase in the corrosion rate for approximately 18 days, after which the mass loss decreased and stabilized. The greatest mass loss of the mixed samples was observed with samples composed of 80Fe-20SS, with an average corrosion rate of 0.17 mm year^{-1}. As the weight percentage of iron decreased (50Fe-50SS and 20Fe-80SS samples), there was a corresponding reduction in the corrosion rate, as shown in Fig. 5b. There was a significant effect of both time and material in the static corrosion tests ($p < 0.0001$ for both, Two Way ANOVA). Stainless steel 316L was significantly different than all amalgamates at all time points ($p < 0.001$, Bonferroni's Multiple Comparison Test).

Galvanic Corrosion Test

Galvanic corrosion tests were conducted in order to assess the galvanic effect of the mixed amalgamates. The method employed measures the galvanic current as a function of time, as presented in Fig. 5c. The corrosion rate was calculated using Eq. (3), and is presented in Fig. 5d. When interpreting the results, it is important to note that the corrosion rate determined is the sole gal-

vanic corrosion rate, and accounts for the additional corrosion created by the resulting galvanic couple.[32] The specimens showed varying amounts of galvanic corrosion. The effect was highest for the 80Fe-20SS/316L couple, with a corrosion rate of approximately 0.48 mm year^{-1}. In comparison, samples composed of 50Fe-50SS and 20Fe-80SS had corrosion rates of approximately 0.26 and 0.070 mm year^{-1}, respectively.

The galvanic corrosion rates were significantly different amongst the tested specimens ($p < 0.0001$, One Way ANOVA). All but the 20Fe-80SS specimen were significantly greater than 316L (for all 50Fe-100Fe specimens: $p < 0.0001$, Bonferroni's Multiple Comparison Test).

Mechanical Test

Micro shear punch tests were conducted, and the resulting force–displacement curves are presented for each trial in Figs. 6a–6c. Deformation and failure behaviour reported from shear punch tests are analogous to that of tensile testing.[21] For all trials, it was evident that the specimens exhibited ductile behaviour until failure. In the majority of the tested specimens, the
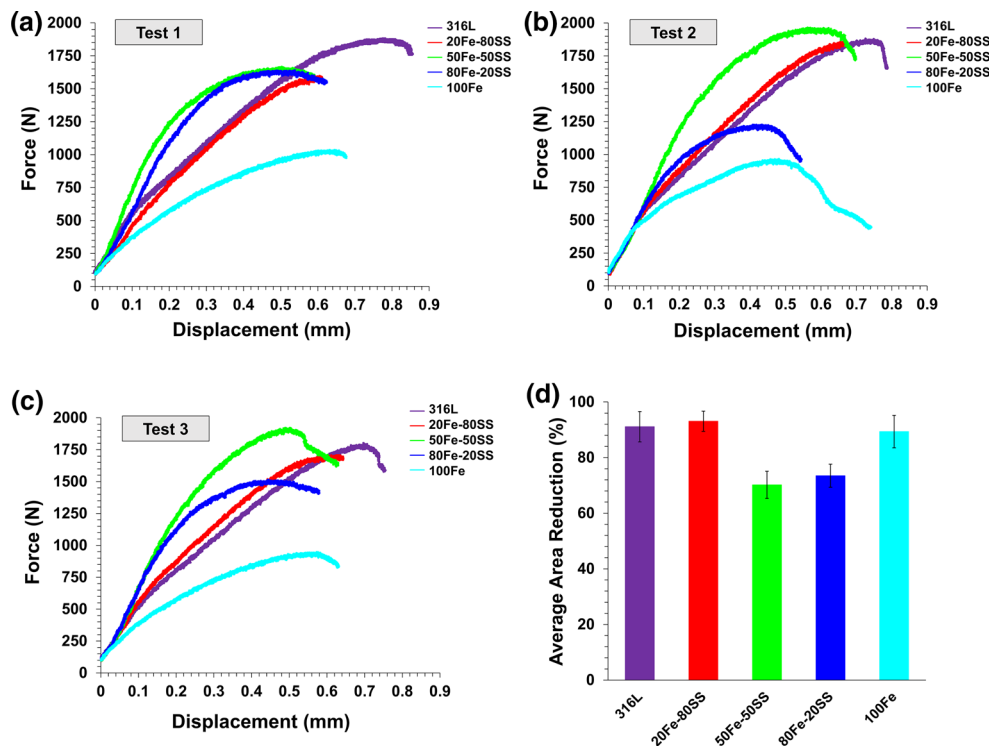
FIGURE 6. Micro-shear punch tests were conducted to assess the mechanical behaviour of the proposed metallic amalgamates. The micro-shear punch tests were completed in triplicate. (a)–(c) Force vs. displacement curves were generated of each trial for the various powder mixtures, with pure stainless steel 316L and iron specimens utilized as a control. (d) In order to assess the ductility of the specimens, the average percent area reduction, with standard deviation, was calculated for each specimen.

mixed amalgamates withstood a maximum force more similar to that of 316L than iron. Furthermore, in two of the three trials, the 50Fe-50SS specimen exceeded the ultimate force withstood by the 316L specimen. The 50Fe-50SS specimens had an average ultimate force 5.5% greater than that of 316L. A similar trend was observed for the required force of fracture, where the majority of the mixed amalgamates fractured at forces more consistent to that of 316L than iron, despite an increasing iron content within the amalgamates.

The average ultimate and fracture forces of the three trials are presented in Table 2, with standard deviation. Interestingly, the increasing weight percentage of iron within the mixtures did not have a substantial impact on the ultimate and fracture forces of the various amalgamates. Overall, there was a significant difference in the fracture force ($p = 0.0007$, One Way ANOVA). Only 100Fe could be isolated as significantly different from 316L ($p < 0.01$, Bonferroni's Multiple Comparison Test). For the ultimate force, a significant difference was determined amongst the mean values ($p < 0.0001$, One Way ANOVA). Again, only 100Fe could be differentiated as significantly different from 316L ($p < 0.001$, Bonferroni's Multiple Comparison Test). The 100Fe specimen was significantly different than 20Fe-80SS, 50Fe-50SS, and 80Fe-

20SS (20Fe-80SS and 50Fe-50SS: $p < 0.01$, 80Fe-20SS: $p < 0.05$, Bonferroni's Multiple Comparison Test).

In order to characterize the expected ductility of the amalgamates, the percent area reduction was determined. This value indicates the specimen's range of ductility, where 0% is brittle and 100% is completely ductile. The results of the calculations are presented in Fig. 6d. Specimens composed of 20Fe-80SS had an average area reduction of $93.1 \pm 3.64\%$, which was greater than that of 316L and 100Fe, which had area reductions of 91.1 ± 5.45 and $89.4 \pm 5.85\%$, respectively. In contrast, 50Fe-50SS and 80Fe-20SS samples had an area reduction approximately 20% less than that of 316L, with respective values of 70.2 ± 4.89 and $73.5 \pm 4.14\%$. Overall, there was a significant difference in the mean area reduction ($p = 0.0018$, One Way ANOVA). The area reduction of the 50Fe-50SS and 80Fe-20SS was significantly less than 316L ($p < 0.05$, Bonferroni's Multiple Comparison Test), however the 20Fe-80SS and 100Fe specimens were not.

Stent Testing

Static Corrosion Test

The corrosion behaviour of the fabricated stent was analyzed using static corrosion tests. The resulting

mass loss curve is presented in Fig. 7a. A rapid increase was observed in the initial corrosion rate for approximately 2 days, with a peak corrosion rate of 0.29 mm year^{-1} determined. The corrosion rate then decreased and stabilized to that of approximately 0.17 mm year^{-1}. An increase in the corrosion rate to 0.27 mm year^{-1} was observed after 7 days, due to localized strut fracture, and therefore, an increase in surface area.

The average corrosion rate, CR$_{static}$, was calculated to be 0.18 ± 0.02 mm year^{-1}. A comparison of the corrosion rate to other degradable metals used in stent application is presented in Table 3. The proposed amalgamate had a degradation rate less than other developing iron-based stents, which had corrosion rates ranging from 0.23 to 0.40 mm year^{-1}, and was closer to that of pure iron (0.20 mm year^{-1}). The proposed amalgamate's corrosion rate was slower than magnesium-based stents, which, for the WE 43 magnesium alloy, was 1.35 mm year^{-1}.[26] In general, the 80Fe-20SS amalgamate had a moderate corrosion rate among other biodegradable stent materials.

The surface morphology of the stent after immersion is presented in Fig. 8. The corrosion progression on the stent surface after 7 days of immersion was evident (Fig. 8b), in comparison to the non-corroded surface (Fig. 8a). A multitude of large dimples was apparent, more so evident at higher magnification (Fig. 8c). Energy dispersive X-ray spectroscopy (EDS) of the degradation layer showed the highest concentration of oxygen in these surface pits, emphasizing the concept that corrosion was aided by surface impurities. EDS analysis also detected significant concentrations of phosphorous, calcium, sodium, and chlorine.

Dynamic Corrosion Test

Dynamic corrosion tests were conducted to analyze the stent's corrosion behaviour in a pseudo-physiological environment (Fig. 1b). The corrosion rate, CR$_{dynamic}$, was calculated to be 0.10 mm year^{-1}. Comparison of CR$_{dynamic}$ to CR$_{static}$ and that of pure iron is presented in Fig. 7b. The dynamic corrosion rate was 42% less than that of CR$_{static}$.

SEM was utilized to characterize the surface morphology of the stent after test completion (Fig. 8). Both the luminal and abluminal surfaces were characterized, in order to account for differences in the degree of corrosion between the surface facing the solution (luminal) and that facing the tubing wall (abluminal). In comparison to the non-corroded surface (Fig. 8d), an array of dimples was evident on both the luminal and abluminal surfaces of the stent (Figs. 8e, 8g). The progression of pitting appeared to be less than that observed from static testing. This was more apparent at higher magnification (Figs. 8f, 8h). When comparing the luminal and abluminal surfaces of the stent however, more significant pitting was observed on the luminal surface, which was directly exposed to the flowing solution. This was further evident through EDS mapping. The iron concentration on the luminal surface was 29.5% less than that observed on the abluminal side of the stent.

TABLE 2. The average ultimate force and fracture force, in *N*, of the various mixed amalgamates.

Specimen type	Average ultimate force (*N*)	Average fracture force (*N*)
316L	1856.7 ± 38.4	1652.4 ± 52.9
20Fe-80SS	1721.7 ± 107.4	1701.5 ± 109.5
50Fe-50SS	1851.7 ± 131.3	1644.7 ± 52.3
80Fe-20SS	1461.8 ± 173.1	1308.2 ± 248.2
100Fe	983.7 ± 38.3	752.5 ± 224.9

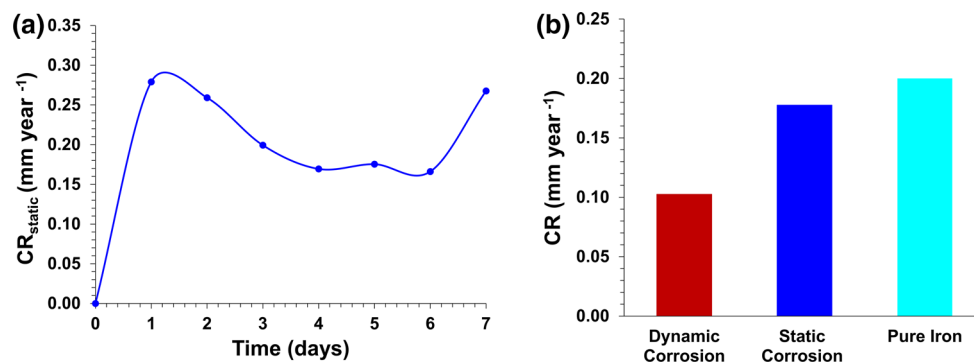Standard deviation is presented, where $n = 3$.

FIGURE 7. (a) A static corrosion test was conducted utilizing a stent specimen. The curve presented shows the change of corrosion rate, in mm year^{-1}, with respect to immersion time. Total test duration was 7 days. (b) A dynamic corrosion test was conducted utilizing a stent specimen in a novel test bench (Fig. 1b). The specimen was removed from the test bench after 7 days, and the corrosion rate was calculated, in mm year^{-1}. It is compared to the static corrosion rate of the stent and that of pure iron. A single stent was utilized for both the static and dynamic corrosion tests.

TABLE 3. Corrosion rates, in mm year^{-1}, for various biodegradable metals used in stent applications.

Material	Corrosion rate (mm year^{-1})	Reference
80Fe-20SS stent (static)	0.18 ± 0.02	–
Pure iron	0.20 ± 0.03	12
Fe-35Mn	0.23 ± 0.03	12
Electroformed iron (E-Fe)	0.40 ± 0.03	27
E-Fe annealed	0.25 ± 0.02	27
Magnesium WE43	1.35*	26
Magnesium cast alloy (AM-60B)	2.78	27

The corrosion rates of the presented materials were obtained under static testing conditions, except for those denoted with an asterisk (magnesium WE43). The degradation rate of magnesium WE43 was determined through potentiodynamic polarization tests.

DISCUSSION

In this work, a novel method was presented to fabricate an Fe-316L metallic stent using CGDS. Mechanical testing and *in vitro* corrosion evaluations indicated that it was a promising technique to develop biodegradable metallic stents with some advantages over currently developed polymer or metallic biodegradable stents.

Cold spray technology is a promising manufacturing method for biodegradable stents, due to a reduction of grain size in the resulting specimen, in the micron to submicron range. Given the recent trend towards decreased strut thickness, small grains are essential in stent design. The resulting improvement of the material's strength, fatigue and wear properties is critical, as device failure due to stent fracture is attributed to high cyclic fatigue, and cold spray processing may alleviate concerns of fatigue-related failure.[1] To assess the grain size of the proposed manufacturing technique, EBSD was conducted utilizing SEM. A flat specimen composed of 316L was analyzed, and small grain sizes were observed (<10 μm).

Clinicians and scientists agree that there are three general requirements for biodegradable stent feasibility: (1) a controlled corrosion rate, with little degradation occurring during vessel remodelling (approximately 6 months),[29] but complete degradation within 12–24 months[30]; (2) mechanical properties that are similar to those of stainless steel 316L, the industry's gold standard for stent design; and (3) stent material that is biocompatible, with degradation products that are non-cytotoxic.

The *in vitro* corrosion behaviour of the proposed amalgamate was assessed utilizing both flat specimens and stents. First, static corrosion tests were conducted of all mixtures to evaluate the resulting corrosion rate.

It was evident that specimens composed of 80Fe-20SS had the greatest corrosion rate of the mixed specimens. The corrosion behaviour of this mixture was further investigated by utilizing stent specimens for static and dynamic corrosion tests.

In comparison to the flat specimens composed of 80Fe-20SS, a similar corrosion rate was observed for the stent sample through static testing (0.18 vs. 0.17 mm year^{-1}). A decrease in the dynamic corrosion rate was observed however, in comparison to the static rate. This is contradictory to the expected corrosion behaviour, as typically the dynamic degradation rate is greater due to the erosion contribution to the overall corrosion mechanism. This difference between the static and dynamic corrosion rates was likely due to the fact that only half of the stent surface was exposed to the flowing corrosive medium, whilst the other half was apposed to the tubing wall. This was further evident when comparing the surface of the stents through EDS. The stent surface after immersion testing had an iron concentration 20.7% less than that observed along the abluminal stent surface after the dynamic corrosion test. The iron concentration along the luminal surface of the stent, however, was more comparable to that determined along the stent surface after static testing (difference < 9%). It is evident that the corrosion behaviour of the stent was influenced by the fact that half of the stent surface was not directly exposed to the corrosive environment. This resulted in an overall decrease in the amount of degradation that occurred.

In addition, the discrepancy between the static and dynamic corrosion tests may also be a result of different testing methodologies. The stent utilized in the static corrosion test was removed from the test bench and cleaned every 24 h. This allowed for a fresh metallic surface to be in contact with the corrosive environment for the duration of the experiment. In contrast, since the stent was crimped and expanded within the tubing of dynamic corrosion test bench, the stent could only be weighed after experiment completion. This allowed a hydroxide layer to form on the surface, which remained for the duration of the test. This likely contributed to the resulting decrease in the dynamic corrosion rate, as the stent was not in direct contact with the HBSS, and Fe^{2+} ions had to diffuse through the hydroxide layer. This phenomenon was further evident when comparing the static and dynamic corrosion specimens through EDS mapping. The luminal stent surface had an oxygen concentration 14.2% greater than that observed along the surface of the static corrosion test specimen.

One of the objectives for the next generation of biodegradable stents is to develop a material with a controllable degradation rate.[26] The benefit of utilizing
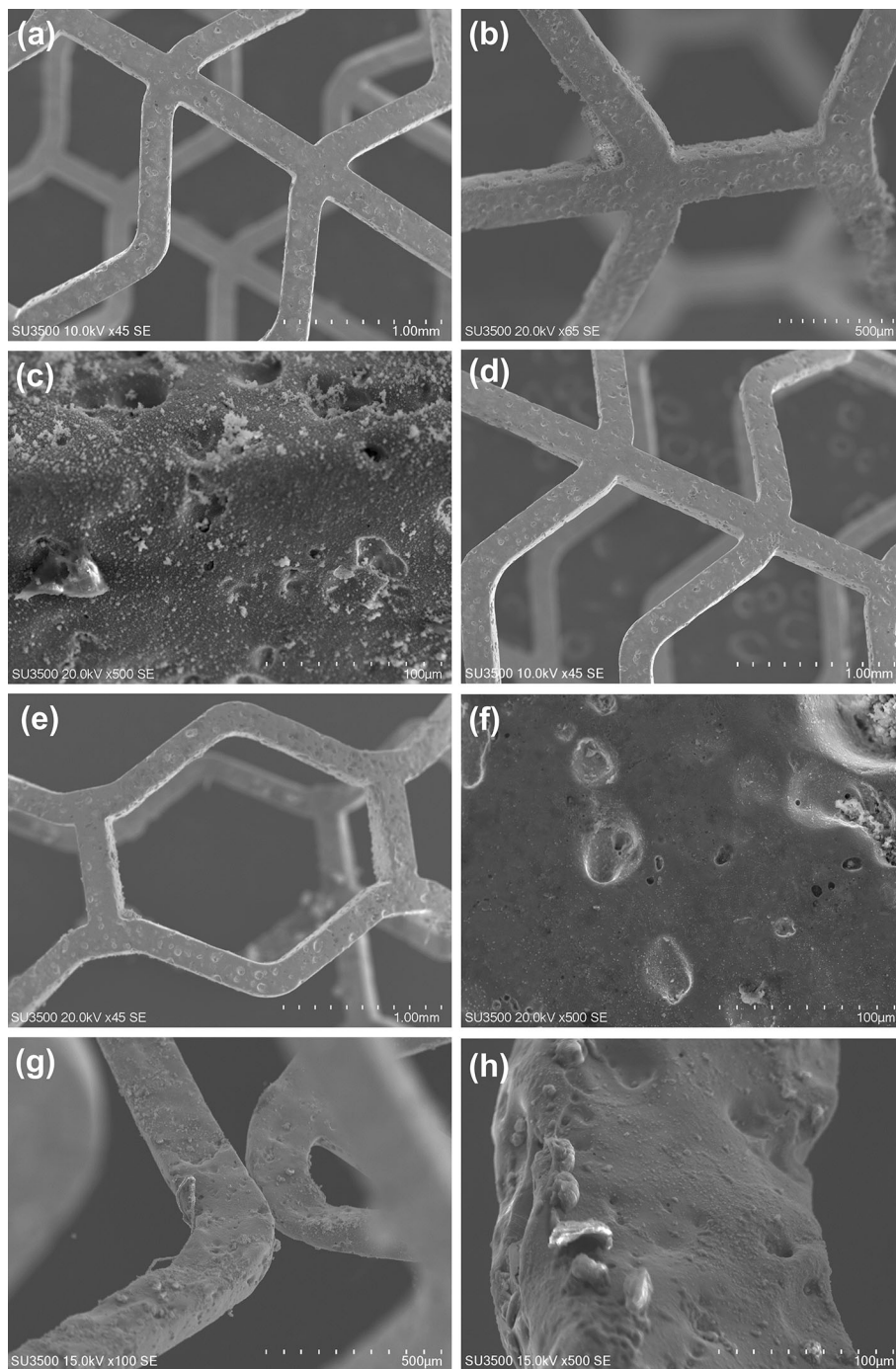
FIGURE 8. Scanning electron microscopy (SEM) was utilized to characterize the surface of the stent prior to and after the static and dynamic corrosion tests. (a) The stent surface prior to static corrosion testing. (b)–(c) The stent surface after test completion, at 65× and 500× magnification, respectively. (d) The surface of the stent prior to dynamic corrosion testing. (e)–(f) The abluminal (external) surface of the stent after 7 days of testing, at 45× and 500× magnification, respectively. (g)–(h) The luminal (internal) surface of the stent after testing, at 100× and 500× magnification, respectively. More significant corrosion can be observed on the luminal surface of the stent, in comparison to the abluminal surface.

two dissimilar metals, like iron and stainless steel 316L, is the ability to control the corrosion rate through the induced galvanic couple. More importantly, due to the homogeneous distribution of the iron and 316L parti-cles (Fig. 2c), the microgalvanic effect can be precisely controlled by modifying the relative percentages of iron and 316L. The loss of material cohesion occurs at a pre-determined rate. In a clinical setting, this can be
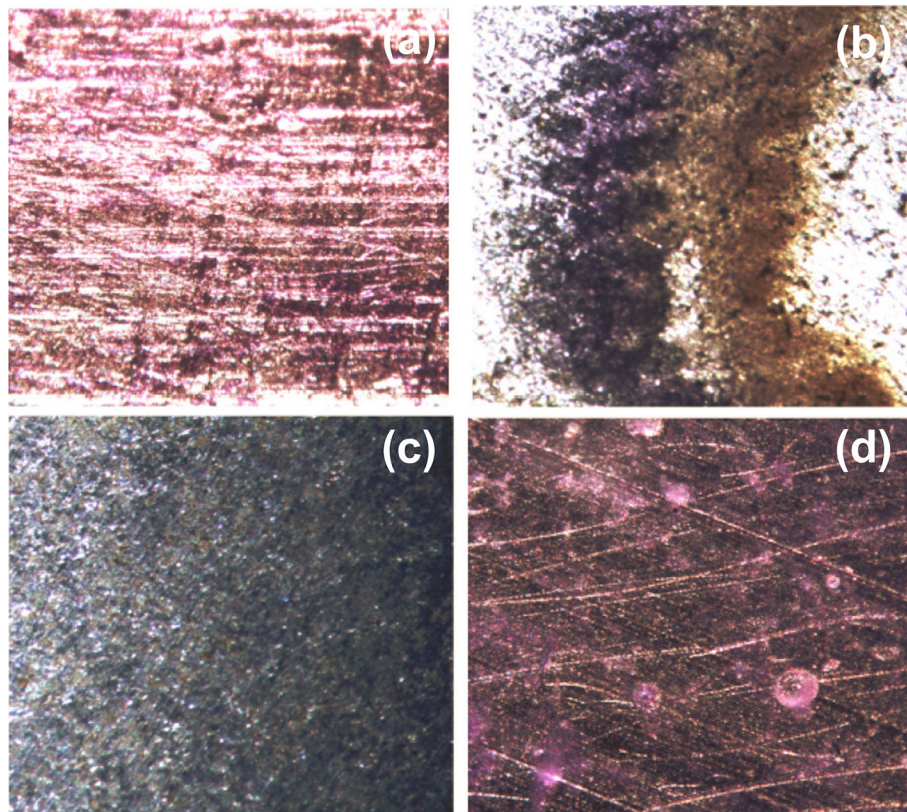
FIG. 9. Endothelial cells with MTT were grown on the surface of a pure 316L specimen (a), implemented as a control, and Fe-316L amalgamates: (b) 20Fe-80SS, (c) 50Fe-50SS, and (d) 80Fe-20SS. Stereo microscopy images were taken specimen surface after 24 h at 225× magnification. Cell growth was observed for all specimens, as indicated by the purple pigmentation of the images

particularly useful, as the corrosion rate of the stent can be tailored to a desired value, based on pre-determined clinical and biological criteria.

Galvanic corrosion tests were conducted to quantify this effect. All samples indicated varying levels of galvanic corrosion, and the effect was highest for the 80Fe-20SS/316L couple. It was evident that bioresorption was further enhanced by microgalvanic effect, in addition to conventional passive oxidation that occurs *in situ*.[18] The overall corrosion rate was accelerated, as multiple corrosion mechanisms contributed to the stent's degradation.

Micro-shear punch tests were conducted to investigate the mechanical behaviour of the proposed amalgamates. The observed deformation and failure behaviour of the mixed specimens were sufficiently ductile, with an area reduction greater than 70% for all specimens. The effect of small grain size was evident during testing, as the ultimate and required fracture forces for the majority of the tested amalgamates was similar to or greater than 316L. Interestingly, the average fracture force of the 80Fe-20SS specimens was more consistent with that of 316L than iron. In particular, in two of the three trials, the 80Fe-20SS amalgamate had an average fracture force only 10%

less than that of 316L. In addition, the average ultimate force of these two trials was only less than 14.4% of 316L. This contradicted the linearity of mixing laws, where it was expected that the ultimate and fracture strengths would be more comparable to that of pure iron. The implication of this finding is that the weight percentage of iron may be further increased in subsequent stents, consequently improving its degradation behaviour without sacrificing the material's mechanical strength. Furthermore, increasing the iron content above 80% may allow for an improved range of ductility, closer to that observed for 100Fe samples from the calculated area reduction.

In vitro corrosion and mechanical evaluations indicated that cold spray technology is a promising technique to develop biodegradable metallic stents. Of the mixed amalgamates investigated, specimens composed of 80Fe-20SS had the best combination of material properties for stent application. Microstructure analysis of the amalgamates indicated similar porosity values for all specimens, with an average porosity of less than 0.31%, which was comparable to 316L. Similarly, ductile deformation and failure behaviour, consistent to that of 316L, was observed for all specimens from shear punch tests. Though 20Fe-80SS and

50Fe-50SS samples had somewhat improved mechanical behaviour over the 80Fe-20SS specimens, their respective degradation rates were too slow for biodegradable stent application. In contrast, the 80Fe-20SS stent had a static degradation rate of 0.18 mm year^{-1}, which is consistent with other developing iron-based stents.

The moderate corrosion behaviour of the 80Fe-20SS amalgamate, enhanced by galvanic effect, makes it a promising candidate for biodegradable stent application. The expected degradation period of the stent can be estimated from the static and dynamic corrosion rates, under similar environmental conditions. Using the static corrosion rate of 0.18 mm year^{-1}, a stent with a mass of 100 mg has an estimated degradation period of approximately 260 days (8.5 months). A 200 mg stent has a predicted survival time of 520 days (17 months). Utilizing the dynamic corrosion rate of 0.10 mm year^{-1}, a 100 mg stent has an estimated degradation time of 390 days (13 months), while a 200 mg stent has a survival period of 780 days (26 months). Since the target degradation period of the stent should be 12–24 months, the estimated survival time of the 80Fe-20SS stent makes it a favourable alternative for biodegradable stent application.

Limitations and Future Work

There are some limitations associated with the present investigations. Given the scope of the tests presented, a minimum number of repetitions were prepared for each investigation. For flat specimen testing, the mechanical and corrosion studies were completed in triplicate. While the sample size was small, consistency within the results was still attained. In future investigations, the number of repetitions will be increased in order to improve reliability. For the static and dynamic corrosion tests utilizing stent specimens, each experiment was performed once, due to the demanding and costly nature of the manufacturing process. This constitutes an important limitation, but a preliminary trend can still be derived from the results. Future work includes additional experiments in order to validate and expand upon the presented results.

The implementation of a pseudo-physiological environment is critical to accurately mimic the degradation process that occurs *in vivo*. For the corrosion tests, the physical reactions that occur on the surface of the stent after implantation, including protein adsorption and cell attachment, were not considered. These processes could slow the stent's overall degradation with time.[33] In addition, stress-facilitated corrosion can affect stent behaviour with time. Additional corrosion investigations should be conducted to investigate the effect of cyclic stresses on stent degradation. In order to obtain a more thorough basis of the material's corrosion properties, future dynamic corrosion tests should also be performed of different durations to assess stent behaviour and to determine when stent fracture and degradation influences the radial stiffness of the stent.

Micro-shear punch tests were conducted to assess the mechanical behaviour of the proposed amalgamates. While shear punch and tensile tests are analogous, the non-uniform deformation zone that results from the shear punch test produces a highly complex stress–strain state. Consequently, the force–displacement curves cannot be utilized to derive the corresponding stress–strain relation. Tensile tests should be conducted for a more comprehensive investigation of the amalgamate's elastic behaviour and tensile properties.

It is known that reduced stent strut thickness may result in statistical size effects, thus affecting mechanical performance. Therefore, the effect of stent structure on the amalgamate's mechanical behaviour should be further assessed. In addition, the effect of degradation on the mechanical performance of the metallic amalgamate was not considered in this work. Future studies will be conducted to take into account corrosion effects on stent mechanical behaviour.

Additional analysis is required to further understand material functionality and viability. Future work should also include more comprehensive dynamic corrosion tests, as well as fatigue testing. Biocompatibility of the proposed amalgamate must also be assessed through *in vitro* and *in vivo* testing. Preliminary biocompatibility studies have been conducted to assess the effect of the proposed amalgamate, and the different mixtures, on endothelialization. Endothelial cells from the human abdominal aortic artery, with added MTT (3-(4,5-dimethylthiazol-2-yl)-2,5-diphenyltetrazolium bromide), were grown on the surface of the specimens (20Fe-80SS, 50Fe-50SS, and 80Fe-20SS), with 316L implemented as a control. Images were taken after 24 h using a stereo microscope at 225× magnification (Fig. 9). Cell growth was observed for all Fe-316L amalgamates, as indicated by the purple pigmentation within the images. In addition, the mitochondrial activity of the Fe-316L specimens was similar to that of the 316L control. While this is a preliminary biocompatibility study, the results demonstrated a certain viability of endothelial cells to grow and proliferate on the proposed amalgamate's surface. More comprehensive *in vitro* and *in vivo* testing are required to fully quantify the proposed invention's biocompatibility.

CONCLUSION

The limitations of current biodegradable stents have resulted in investigations into novel biomaterials for stent application. Innovative alloys, improved microstructure, and novel manufacturing techniques are required for the implementation of biodegradable stents in the global market. The subsequent generation of biodegradable stents has focused on material optimization, with sustained mechanical integrity and a controllable degradation rate.

Therefore, a newly developed metallic, nano-structured material for stent application was presented, fabricated through a novel application of CGDS. Cold spray allows for the manufacturing of materials with very small grain size, resulting in improved mechanical properties and fatigue resistance. Materials composed of varying proportions of iron and stainless steel 316L were investigated, in order to determine the ideal amalgamate. Mechanical and *in vitro* corrosion tests were conducted to analyze the materials. Shear punch tests demonstrated mechanical behaviour comparable to that of stainless steel 316L. The corrosion behaviour of the amalgamate was enhanced and accelerated due to microgalvanic effect. As a result, the corrosion rate can be controlled by the relative percentage of the powders. Moreover, it was found that while increasingly the relative iron content of the amalgamate improved the corrosion rate, it also maintained mechanical behaviour consistent to that of 316L, which cannot be extrapolated from proportional mixing laws. This may allow for an increase of the iron within the amalgamate to greater than 80%, further improving the corrosion behaviour, without sacrificing the mechanical properties of the stent.

It was shown that the proposed manufacturing technique utilizing CGDS is a promising approach for stent fabrication, and provides a different paradigm than other reactive metals for developing biodegradable stent materials. The investigations conducted indicated that specimens composed of 80% iron and 20% stainless steel 316L had the most effective combination of mechanical and corrosion properties for biodegradable stent application.

ACKNOWLEDGMENTS

REFERENCES

[1] Al-Mangour, B. The use of cold sprayed alloys for metallic stents. Master's of Engineering, Department of Mechanical Engineering, McGill University, Montreal, Canada, 2012.

[2] Al-Mangour, B., R. Mongrain, E. Irissou, and S. Yue. Improving the strength and corrosion resistance of 316L stainless steel for biomedical applications using cold spray. *Surf. Coat. Technol.* 216:297–307, 2013.

[3] ASTM G31-12a. Standard Guide for Laboratory Immersion Corrosion Testing of Metals. West Conshohocken, PA: ASTM International, 2012. doi:10.1520/G0031-12A.

[4] ASTM G71-81. Standard Guide for Conducting and Evaluating Galvanic Corrosion Tests in Electrolytes. West Conshohocken, PA: ASTM International, 2014. doi:10.1520/G0071.

[5] Barua, R. Study of the structural properties and control of degradation rate for biodegradable metallic stents using cold spray. Doctor of Philosophy, Department of Mechanical Engineering, McGill University, Montreal, Quebec, 2015.

[6] Bertrand, O. F., R. Sipehia, R. Mongrain, J. Rodés, J. C. Tardif, L. Bilodeau, G. Côté, and M. G. Bourassa. Biocompatibility aspects of new stent technology. *J. Am. Coll. Cardiol.* 32(3):562–571, 1998.

[7] Champagne, V. K. The Cold Spray Materials Deposition Process: Fundamentals and Applications. Cambridge: Woodhead Publishing, 2007.

[8] Drynda, A., T. Hassel, F. W. Bach, and M. Peuster. In vitro and in vivo corrosion properties of new iron–manganese alloys designed for cardiovascular applications. *J. Biomed. Mater. Res. B Appl. Biomater.* 103(3):649–660, 2015.

[9] Francis, A., Y. Yang, S. Virtanen, and A. R. Boccaccini. Iron and iron-based alloys for temporary cardiovascular applications. *J. Mater. Sci. Mater. Med.* 26(3):1–16, 2015.

[10] Geers, M. G. D., W. A. M. Brekelmans, and P. J. M. Janssen. Size effects in miniaturized polycrystalline FCC samples: strengthening versus weakening. *Int. J. Sol. Struct.* 43(24):7304–7321, 2006.

[11] Henning, M., and V. Horst. Statistical size effects based on grain size and texture in thin sheets. *Mater. Sci. Eng. A.* 452(1):602, 2007.

[12] Hermawan, H. Biodegradable Metals: From Concept to Applications. Berlin: Springer, pp. 49–57, 2012.

[13] Hermawan, H., D. Dube, and D. Mantovani. Degradable metallic biomaterials: design and development of Fe-Mn alloys for stents. *J. Biomed. Mater. Res. A.* 93(1):1–11, 2010.

[14] Hermawan, H., D. Dubé, and D. Mantovani. Degradable metallic biomaterials for cardiovascular applications. In: Metals for Biomedical Devices, edited by M. Niinomi. Cambridge: Woodhead Publishing, 2010, pp. 379–404.

[15] Heublein, B., R. Rohde, V. Kaese, M. Niemeyer, W. Hartung, and A. Haverich. Biocorrosion of magnesium

alloys: a new principle in cardiovascular implant technology? *Heart* 89(6):651–656, 2003.

[16] Huang, T., J. Cheng, D. Bian, and Y. Zheng. Fe–Au and Fe–Ag composites as candidates for biodegradable stent materials. *J. Biomed. Mater. Res. B Appl. Biomater.* 2015. doi:10.1002/jbm.b.33389.

[17] Jukema, J. W., T. A. N. Ahmed, J. J. W. Verschuren, and P. H. A. Quax. Restenosis after PCI. Part 2: prevention and therapy. *Nat. Rev. Cardiol.* 9(2):79–90, 2012.

[18] Kalb, H., A. Rzany, and B. Hensel. Impact of microgalvanic corrosion on the degradation morphology of WE43 and pure magnesium under exposure to simulated body fluid. *Corros. Sci.* 57:122–130, 2012.

[19] Kastrati, A., J. Mehilli, J. Dirschinger, F. Dotzer, H. Schühlen, F. J. Neumann, M. Fleckenstein, C. Pfafferott, M. Seyfarth, and A. Schömig. Intracoronary stenting and angiographic results: strut thickness effect on restenosis outcome (ISAR-STEREO) trial. *Circulation* 103(23):2816–2821, 2001.

[20] Kirkland, N. T., N. Birbilis, and M. P. Staiger. Assessing the corrosion of biodegradable magnesium implants: a critical review of current methodologies and their limitations. *Acta Biomater.* 8(3):925–936, 2012.

[21] Lucas, G. E., G. R. Odette, and J. W. Sheckherd. Shear punch and microhardness tests for strength and ductility measurements. In: Use of Small-Scale Specimens for Testing Irradiated Material, edited by W. R. Corwin, and G. Lucas. Philadelphia, PA: American Society for Testing and Materials (ASTM), 1986, pp. 112–140.

[22] Miyazaki, S., K. Shibata, and H. Fujita. Effect of specimen thickness on mechanical properties of polycrystalline aggregates with various grain sizes. *Acta Metall.* 27(5):855–862, 1979.

[23] Mongrain, R., E. Aboumansour, S. Plante, O. F. Bertrand, and J. C. Tardif. Development of a 3D CAD model for the structural analysis of a coronary stent. In: International Symposium on Advanced Materials for Biomedical Applications (SAMBA), edited by D. Mantovani. Montreal: The Canadian Institute of Mining, Metallurgy and Petroleum, 2002.

[24] Mongrain, R., O. F. Bertrand, and S. Yue. Bioresorbable Medical Devices and Method of Manufacturing the Same. USPTO, WO 2013163747 A1, 2013.

[25] Moore, J., J. Soares, and K. Rajagopal. Biodegradable stents: biomechanical modeling challenges and opportunities. *Cardiovasc. Eng. Technol.* 1(1):52–65, 2010.

[26] Moravej, M., and D. Mantovani. Biodegradable metals for cardiovascular stent application: interests and new opportunities. *Int. J. Mol. Sci.* 12(7):4250–4270, 2011.

[27] Moravej, M., A. Purnama, M. Fiset, J. Couet, and D. Mantovani. Electroformed pure iron as a new biomaterial for degradable stents: in vitro degradation and preliminary cell viability studies. *Acta Biomater.* 6(5):1843–1851, 2010.

[28] Murphy, B. P., P. Savage, P. E. McHugh, and D. F. Quinn. The stress-strain behavior of coronary stent struts is size dependent. *Ann. Biomed. Eng.* 31(6):686–691, 2003.

[29] Schomig, A., A. Kastrati, H. Mudra, R. Blasini, H. Schuhlen, V. Klauss, G. Richardt, and F. J. Neumann. Four-year experience with Palmaz-Schatz stenting in coronary angioplasty complicated by dissection with threatened or present vessel closure. *Circulation* 90(6):2716–2724, 1994.

[30] Serruys, P. W., M. J. Kutryk, and A. T. Ong. Coronary-artery stents. *N. Engl. J. Med.* 354(5):483–495, 2006.

[31] Simsekyilmaz, S., E. A. Liehn, C. Militaru, and F. Vogt. Progress in interventional cardiology: challenges for the future. *Thromb. Haemost.* 113(3):464–472, 2015.

[32] Baboian, R. Corrosion Tests and Standards: Application and Interpretation (2nd ed.). West Conshohocken, PA: ASTM International, 2005. ISBN 978-0-8031-4555-9.

[33] Zhen, Z., T.-F. Xi, and Y.-F. Zheng. A review on in vitro corrosion performance test of biodegradable metallic materials. *Trans. Nonferr. Met. Soc. China.* 23(8):2283–2293, 2013.